Journal of Materials Chemistry A

Alkaline Salt-Promoted Construction of Hydrophilic and Nitrogen Deficient Graphitic Carbon Nitride with Highly Improved Photocatalytic Efficiency

Journal:	*Journal of Materials Chemistry A*
Manuscript ID	TA-COM-01-2021-000524
Article Type:	Communication
Date Submitted by the Author:	19-Jan-2021
Complete List of Authors:	Chen, Hao; The University of Tennessee, Department of Chemistry Wang, Wuyou; Nanchang University Yang, Zhenzhen; Oak Ridge National Laboratory, Chemical Science Division Suo, Xian; University of Tennessee Knoxville Lu, Ziyang; Jiangsu University, School of the Environment and Safety Engineering, Institute of Environmental Health and Ecological Security Xiao, Weiming; Nanchang University, Department of Chemistry Dai, Sheng; Oak Ridge National Laboratory,

SCHOLARONE™
Manuscripts

Journal Name

COMMUNICATION

Alkaline Salt-Promoted Construction of Hydrophilic and Nitrogen Deficient Graphitic Carbon Nitride with Highly Improved Photocatalytic Efficiency

Received 00th January 20xx,
Accepted 00th January 20xx

DOI: 10.1039/x0xx00000x

www.rsc.org/

Hao Chen [a, +], Wuyou Wang [c, +], Zhenzhen Yang [b *], Xian Suo [a], Ziyang Lu [a, e], Weiming Xiao[d] and Sheng Dai [a,b *]

Graphitic carbon nitride (g-C_3N_4) possesses fascinating merits, but its practical applications are limited by the inferior properties of limited visible-light sorption, rapid recombination of photo-excited charge carriers and low electrical conductivity. Introduction of N-defects is an efficient approach to tune its optical properties, but strategies capable of creating abundant vacancies and simultaneously maintaining the highly crystalline architecture are still limited and highly desired. In this work, a facile construction methodology was demonstrated to afford g-C_3N_4 with abundant N vacancies, high crystallinity, hydrophilic surface structure, small particle size, and increased surface area under neat and mild conditions. The essence of our approach lies in the treatment of bulk g-C_3N_4 precursor by an alkaline salt ($LiN(SiMe_3)_2$) with a low melting point, moderate nucleophilicity, and easy removal procedure. The unique structural properties of the afforded ND-g-C_3N_4 allow for a significantly redshifted absorption edge and enhanced charge carrier separation, leading to superior photocatalytic hydrogen evolution performance three times that obtained by the pristine g-C_3N_4. The modification strategy developed herein sheds light on the fabrication of g-C_3N_4-based materials with improved photocatalytic efficiency via efficient introduction of N defects, variation of the surface structure, and retention of the high crystallinity.

Two-dimensional (2D) nanomaterials possessing sheet-like structures have electron confinement in two dimensions and feature unique physical, chemical, optical, and electronic properties.[1-4] Their explorations are growing rapidly in the fields of physics, material science, chemistry, and nanotechnology.[5-8] Particularly, precise control on the crystallinity, thickness, defects, surface compositions, etc. could achieve fine tuning of the performance and offer new opportunities to extend their practical applications.[1, 9-12] Graphitic carbon nitride (g-C_3N_4) is an analogue of graphite constructed by van der Waals layered structures composed of *sp*^{2} hybridized carbon and nitrogen atoms.[13-18] Bulk g-C_3N_4 powder could be obtained via thermal treatment of cost-effective and abundant nitrogen-rich resources including melamine,[6, 19, 20] urea,[21] cyanamide,[22] dicyandiamide,[23] ammonium thiocyanate[24] and so on. Besides their advantages of nontoxicity, easy preparation, and low cost, they have demonstrated fascinating merits lying in proper electronic band structure, moderate bandgap, and good stability (e.g., thermally stable up to 600 °C in air). All these desirable attributes make them promising candidates in photocatalysis[25], which has been witnessed by numerous research endeavours since the pioneer work by Wang et al. in 2009 towards the photocatalytic H_2 evolution promoted by metal-free semiconductor g-C_3N_4.[26, 27] Starting from H_2 production[28, 29], their photocatalytic utilization has been extended to various processes in water oxidation,[30] CO_2 reduction,[31, 32] artificial photosynthesis,[33] and organic pollutant degradation.[34, 35] However, limited visible-light sorption range of the pristine g-C_3N_4 (lack of absorption above 460 nm) as well as the rapid recombination of the generated photo-excited charge carriers and low electrical conductivity led to inferior photocatalytic performance.[36] To remove these obstacles and shortcomings, surface modification treatments were performed to regulate the nanostructure of g-C_3N_4 towards extending the light absorption region, retarding the recombination of photoinduced charge carriers, and enhancing the surface affinity to the reactant species. The electronic structure and energy band configuration of g-C_3N_4 matrix can be modified by introducing impurities into the skeleton through the copolymerization and doping procedures.[37, 38] Morphologies of g-C_3N_4 can be engineered by adding soft or hard template, supramolecular preorganization, and exfoliation, affording various geometrical shapes with tunable lateral size and improved photoelectric properties.[39-41] Formation of g-C_3N_4-based heterojunctions is also capable of remarkably enhancing the photocatalytic activity for task-specific applications.[13, 42]

Recently, the introduction of defects within the skeleton of g-C_3N_4 was demonstrated to play a significant role in modifying its photoelectric properties, which could act as trapping sites for

[a]Department of Chemistry, The University of Tennessee, Knoxville, TN, 37996, United States.
[b]Chemical Sciences Division, Oak Ridge National Laboratory, Oak Ridge, TN 37831, United States.
[c] School of Chemistry & Chemical Engineering, Yancheng Institute of Technology, Yancheng, 224051, P. R. China.
[d] Institute of Applied Chemistry, College of Chemistry, Nanchang University, Nanchang, Jiangxi 330031, P. R. China.
[e] School of the Environment and Safety Engineering, Institute of Environmental Health and Ecological Security, Jiangsu University, Jiangsu, Zhenjiang, 212013, China.

[+] These authors contributed equally.
Corresponding authors: zyang17@utk.edu (Z. Yang), dais@ornl.gov (S. Dai)
Electronic Supplementary Information (ESI) available: [details of any supplementary information available should be included here]. See DOI: 10.1039/x0xx00000x

This journal is © The Royal Society of Chemistry 20xx

Please do not adjust margins

photoinduced carriers, thus slowing down the recombination of holes and electrons and enhancing the overall quantum efficiency.[37] Using dicyandiamide as the precursor, N vacancies in the framework of g-C_3N_4 could be created by increasing the polycondensation temperature from 550 to 600 °C, affording g-C_3N_4 with enhanced photocatalytic efficiency in radical generation, Rhodamine B decomposition, and hydrogen evolution.[43] Hydrothermal treatment of the pristine g-C_3N_4 in the presence of ammonium thiosulfate (oxidant) led to the formation of nitrogen-deficient g-C_3N_4 with broadened visible-light absorption.[37] Niu et al. demonstrated a H_2 reduction approach to create nitrogen vacancies within the framework of g-C_3N_4 by removal of 7% nitrogen atoms from the bulk precursor.[44] However, in these procedures, control intensity over the abundance and type of the defects was limited owing to the relatively weak interaction between the additives/gaseous atmosphere with the g-C_3N_4 layers. In order to enhance the vacancy creation efficiency from the parent g-C_3N_4, Mg was added to catalyze the denitriding process via thermal treatment at 750 °C, and the nitrogen content of g-C_3N_4 was dramatically dropped from 57.1 to 8.84 at.%.[45] However, the afforded defective g-C_3N_4 was black powder and apparently possessed no photocatalytic activity. Cu powder and Fe powder were also efficient for this purpose but with the same issues derived from the strong catalytic activities for C–N bond cleavage, alternatively producing N-doped carbon used as organic anode material in Lithium ion battery.[46] The group of Zhang developed a KOH-assisted route to fabricate defective g-C_3N_4 by tuning the ratio of KOH: urea.[40] Redshift of the g-C_3N_4 absorption edge was achieved with gradually increased KOH dosage. However, the ordered structure of g-C_3N_4 framework was lost during the thermal polymerization procedure. Notably, the highly crystalline architecture within the g-C_3N_4 nanosheets plays important roles in facilitating the electron transfer process.[41, 47] Therefore, it is still highly desired and challenging to find a facile and efficient pathway capable of producing g-C_3N_4 with abundant and tunable vacancy regulation while simultaneously maintaining the high crystallinity to afford improved photocatalytic efficiency.

In this work, a facile construction methodology was demonstrated to afford g-C_3N_4 with abundant N vacancies, high crystallinity, hydrophilic surface structure, small particle size, and increased surface area under neat and mild conditions (Figure 1A). The essence of our approach lies in the treatment of bulk g-C_3N_4 precursor by an alkaline salt ($LiN(SiMe_3)_2$) with low melting point, moderate nucleophilicity, and easy removal procedure. The unique structural properties of the afforded ND-g-C_3N_4 provide it with significantly redshifted absorption edge and enhanced charge carrier separation, leading to superior photocatalytic hydrogen evolution performance three times that obtained by the pristine g-C_3N_4. The modification strategy developed herein sheds light on the fabrication of g-C_3N_4-based materials with improved photocatalytic efficiency via efficient introduction of N defects, variation of the surface structure, and retention of the high crystallinity.

The chemical structure of g-C_3N_4 is mainly composed of heptazine units connected by polar C–N and C=N bonds.[33] The involvement of electron-withdrawing (C) and electron-donating sites (N) offered opportunities for the exfoliation and modification of the 2D g-C_3N_4 nanosheets by ion pair-containing reagents performing enhanced intercalation between the layered structures. For example, exfoliation of bulk g-C_3N_4 in acid or alkaline medium could efficiently afford ultra-thin g-C_3N_4 sheets with small sized fragments.[48] KOH showed the ability to generate vacancies within the g-C_3N_4 framework, but its melting point was relatively high (360 °C), so thermal treatment process at high temperatures was required, and its basicity was too strong leading to collapse of the crystalline architecture to some extent, with g-C_3N_4 being obtained as amorphous or low crystalline counterpart.[40] To take advantage of the alkaline salts in creating defects within the g-C_3N_4 backbone and simultaneously retaining the high crystallinity of the material, cost-effective alkaline salts with low melting point, capability to cleave C–N or C=N bonds, and complete removal through easy-handling procedure are preferred. Towards these considerations, commercially available lithium bis(trimethylsilyl)amide (LiHMDS) was adopted as the solvent and catalyst for the fabrication of g-C_3N_4 with red-shifted absorption edges induced by vacancy formation. The potential merit of using LiHMDS (Table S1) lies in (1) low melting point (71 °C) allowing treatment under neat and relatively mild condition, (2) moderate basicity (pK_a = 26) allowing for suitable bond cleavage ability, (3) decomposition in H_2O and high solubility in most aprotic organic solvents (e.g., tetrahydrofuran, hexane, and toluene) leading to easy removal from the resultant g-C_3N_4 and ensuring the purity of the product.

As an initial assessment of the possiblity to construct nitrogen deficient g-C_3N_4 in the presence of LiHMDS, the parent g-C_3N_4 was prepared from urea at 550 °C via a previously reported procedure,[49] resulting in a light yellow solid. A mixture of the bulk g-C_3N_4 and LiHMDS was ground uniformly, which was then treated under N_2 atmosphere at 250 °C for 24 h. Then, the alkaline salt was removed by a washing procedure, and the g-C_3N_4 product (denoted as ND-g-C_3N_4) was collected as a brown powder (Figure 1A). For comparison, the structures of the g-C_3N_4 precursor and the ND-g-C_3N_4 product were characterized by X-ray diffraction (XRD) patterns, Fourier transform infrared (FTIR) spectroscopy, and X-ray photoelectron spectroscopy (XPS) measurements. In the XRD pattern of the pristine g-C_3N_4, two characteristic peaks located at 13.3° and 27.7° appeared, being assigned to the (100) and (002) crystal planes, respectively (Figure 1B).[15] That is, the hole-to-hole distance for the in-plane structural packing motif was 0.68 nm and interlayer spacing for the interfacial stacking of the sheets was 0.33 nm. Comparatively, after thermal treatment by LiHMDS, the (002) crystal plane of the produced ND-g-C_3N_4 still located at 27.7°, indicating that the interlayer distance was maintained well and no collaspe of the architecture was observed. However, the characteristic peak of the (100) crystal plane shifted to 11.7°, which demonstrated an increased hole-to-hole distance (0.79 nm) owing to the formation of nitrogen vacancies. In the FTIR spectra (Figure 1C), for g-C_3N_4 before and after treatment by LiHMDS, characteristic peak for the out-of-plane bending mode of heptazine units was shown up at 810 cm^{-1}, together with typical signals for the N–C=N heteroaromatic rings within the framework at 880–1630 cm^{-1}.[40] The intensity of N–H stretching vibrations corresponding to the broad peak around 3175 cm^{-1} was significantly increased in the spectrum of ND-g-C_3N_4, indicating the involvement of more N–H moieties, which may influence its physical properties. XPS measurements verified the successful introduction of surface N defects within the backbone of ND-g-C_3N_4, as the N content decreased from 38.4 at.% in pristine g-C_3N_4 to 18.6 at.% (Figure S1). C1s XPS spectrum of the pristine g-C_3N_4 can be resolved to three peaks with binding energies (BEs) of 284.5, 285.8 and 287.9 eV, being assigned to N–C=N coordination, C–NH_x/C-O bonds, and adventitious C–C bonds, respectively (Figure 1D).[40] These three peaks also presented in the C1s spectrum of ND-g-C_3N_4 with higher ratio of C-NH_x/C-O bonds (21%) than that in g-C_3N_4 (8%) (Figure 1E), which was consistent with the FTIR results by the enhanced N–H absorption intensity in

This journal is © The Royal Society of Chemistry 20xx

Please do not adjust margins

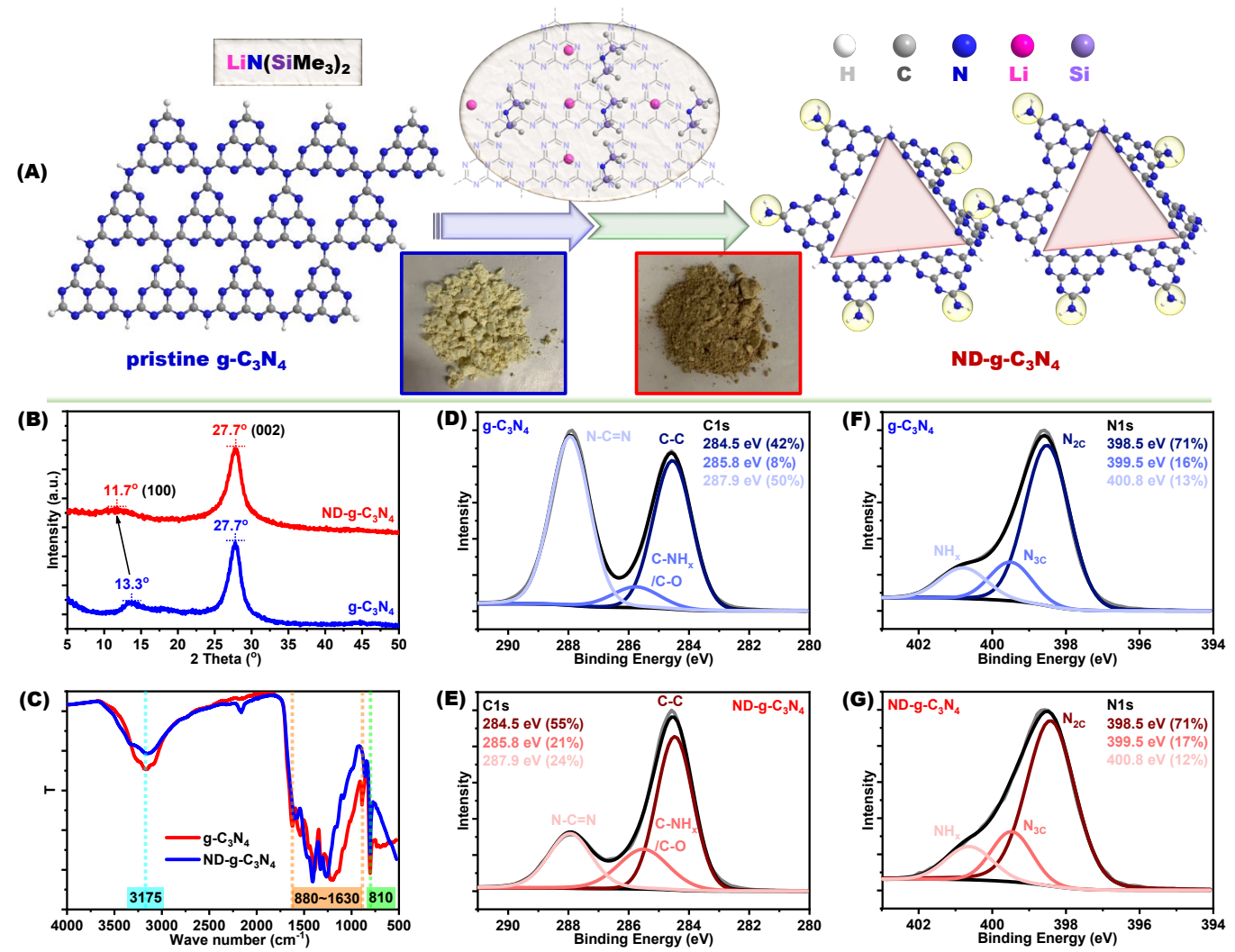

Figure 1. (A) Schematic diagram for the fabrication of ND-g-C_3N_4 in the presence of $LiN(SiMe_3)_2$. Pictures in the blue and red box were powder of g-C_3N_4 precursor and the ND-g-C_3N_4 product, respectively. (B) XRD patterns, (C) FTIR spectra, (D, E) C1s XPS spectra, and (F, G) N1s XPS spectra of g-C_3N_4 precursor and the ND-g-C_3N_4 product.

ND-g-C_3N_4 (Figure 1C). The presence of three N species including bicoordinated (N_{2C}), tricoordinated (N_{3C}) forms, and NH_x groups was demonstrated in the N1s spectrum of g-C_3N_4, with BEs of 398.5, 399.5, and 400.8 eV, respectively (Figure 1F). All these N-containing functionalities were still retained in the framework of ND-g-C_3N_4 with very close ratios (Figure 1G). These results indicated that after treating by LiHMDS, the N vacancies were mainly formed by the cleavage of C–NH_x bonds within the center of the backbone, which were reconstructed at the edge of the framework owing to the strong nucleophilicity of the $^-N(SiMe_3)_2$ anion and the existence of electro-deficient carbons on the edge sites. Besides, the afforded ND-g-C_3N_4 exhibited relatively higher O content (11.7 at.%) compared with that in the g-C_3N_4 precursor (4.5 at.%), which was probably introduced by the hydrolysis of LiHMDS. However, the property variation of the material was still dominated by the significant difference of N-containing moieties. The electron paramagnetic resonance (EPR) spectra of g-C_3N_4 and ND-g-C_3N_4 demonstrated that after treatment by LiHMDS, a considerable amount of of unpaired electrons were introduced, which were mainly localized within the skeleton of ND-g-C_3N_4, as indicated by the symmetric shape of the spectra (Figure S2). The structure characterizations demonstrated that N defects were successfully created in the center region of the ND-g-C_3N_4 nanosheets together with the presence of abundant NH_x groups on the edge sites. Thermogravimetric analysis (TGA) was conducted to evaluate the thermal stability of the as-prepared materials (Figure S3). The results showed that under N_2 atmosphere, the onset decomposition temperature of ND-g-C_3N_4 was 430 °C, while that of the g-C_3N_4 precursor was 540 °C, which was due to the formation of some small segments derived from the cleavage of C-N bond during the treatment by LiHMDS.

In order to gain insight into the physical property variation derived from the increased content of NH_x moieties, water contact angles of the pristine g-C_3N_4 and the afforded ND-g-C_3N_4 were measured. As shown in Figure 2A and 2B, a significant decrease of the water contact angle from 52.3° to 31.0° was obtained after treatment by LiHMDS, indicating the enhanced hydrophilicity of ND-g-C_3N_4 induced by more hydrogen bonding formation, which will bring benefits for photocatalytic procedures in aqueous media. Scanning electron microscopy (SEM) and transmission electron microscopy (TEM) images were collected and compared to illustrate

Please do not adjust margins

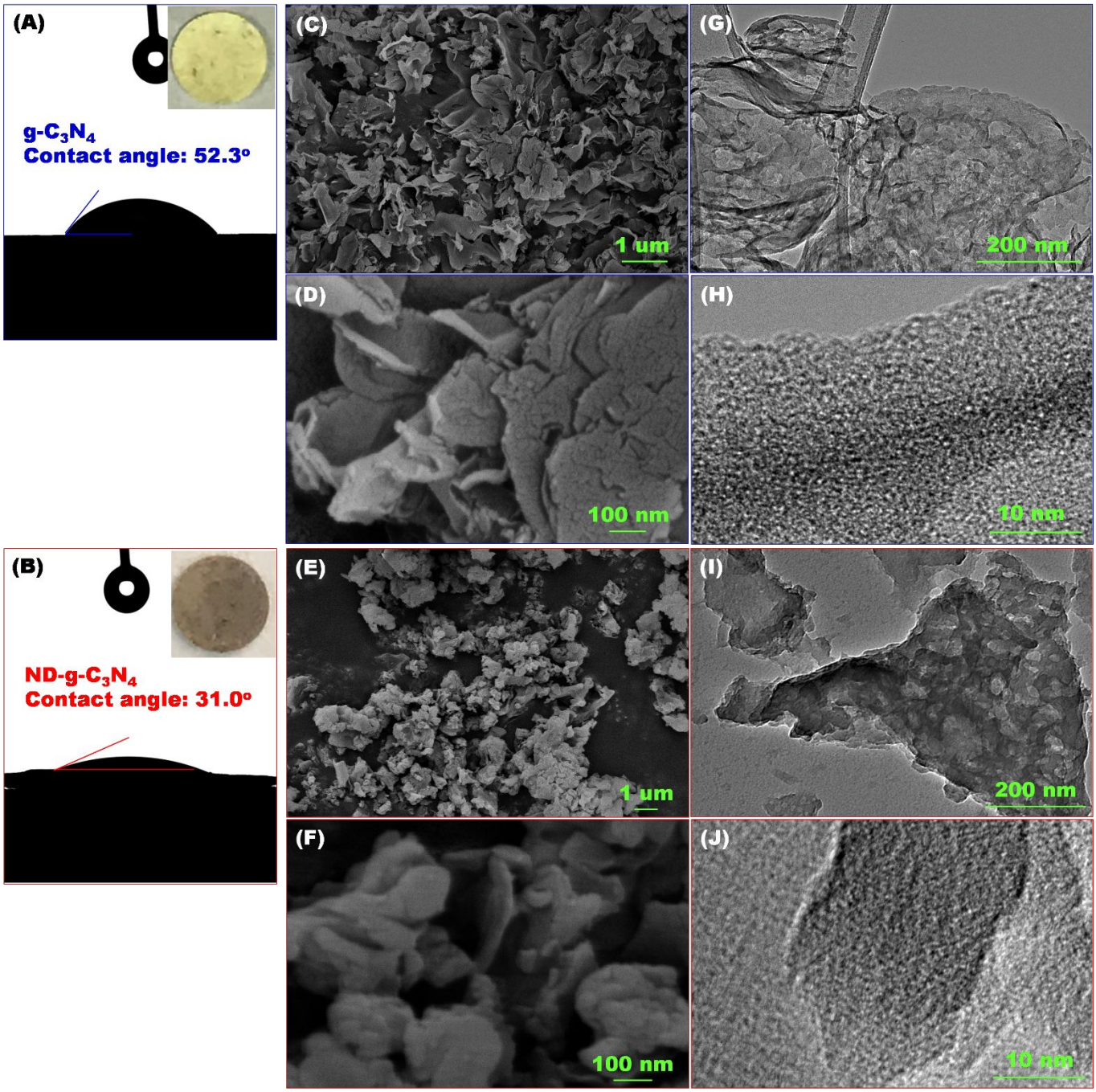

Figure 2 (A, B) Optical photographs for the water contact angle measurement for g-C_3N_4 precursor and ND-g-C_3N_4 product. A sessile water droplet of 2.0 μL was added. Inset pictures are the dense sheet of the samples with flat surface. (C, D) SEM images of g-C_3N_4 precursor and (E, F) ND-g-C_3N_4 product. (G, H) TEM images of g-C_3N_4 precursor and (I, J) ND-g-C_3N_4 product.

the morphology change. SEM images of the pristine g-C_3N_4 (Figure 2C and 2D) showed that it was composed of films with large area size (>500 nm) and thickness. Comparatively, the ND-g-C_3N_4 product exhibited particle morphology with much smaller particle size (~200 nm) (Figure 2E and 2F), which can be homogeneously and stably dispersed in the reaction mixtures. TEM images of the pristine g-C_3N_4 (Figure 2G and 2H) were in accordance with the large film-type structure and that of the ND-g-C_3N_4 product confirmed the particle morphology with permanent porosity within the structures (Figure 2I and 2J). Correspondingly, the Brunauer–Emmett–Teller (BET) specifc surface area of the as-prepared ND-g-C_3N_4 increased to 30 m^2 g^{-1}, while that of the pristine g-C_3N_4 was 8 m^2 g^{-1}, due to the formation of extra vacancies and the small particle morphology, as calculated from the N_2 adsorption isotherms at 77 K (Figure S4). Notably, the quality of the ND-g-C_3N_4 was significantly influenced by the reaction time, thermal treatment temperature, and dosage of the LiHMDS. When the g-C_3N_4 precursor was treated at 250 °C for 6 h (Figure S5), some impurities

This journal is © The Royal Society of Chemistry 20xx

Please do not adjust margins

derived from depolymerization of the backbone were detected by XRD and the characteristic peak for the (100) crystal plane was broad with weak intensity, indicating that the vacancies were still small with low content. The purity of the product was slightly improved by prolonging the reaction time to 12 h, and ND-g-C_3N_4 with abundant N vacancies and high crystallinlty was obtained after treatment for 24 h. Vacancies were already formed by treatment of the g-C_3N_4 precursor at 150 °C together with the involvement of some impurities (Figure S6). 250 °C was the optimum temperature and further increasing the temperature to 350 °C led to the collapse of the architecture as reflected by the broadened peak for (002) crystal plane. In addition, enough LiHDMS was required for homogeneous dispersion of the g-C_3N_4 precursor to afford the product with rich defects (Figure S7).

The combination of the features including abundant N defects, enhanced hydrophilicity, small particle size composition, and increased surface area will give the resultant ND-g-C_3N_4 material improved optical and electronic properties. First, the UV-Vis diffuse

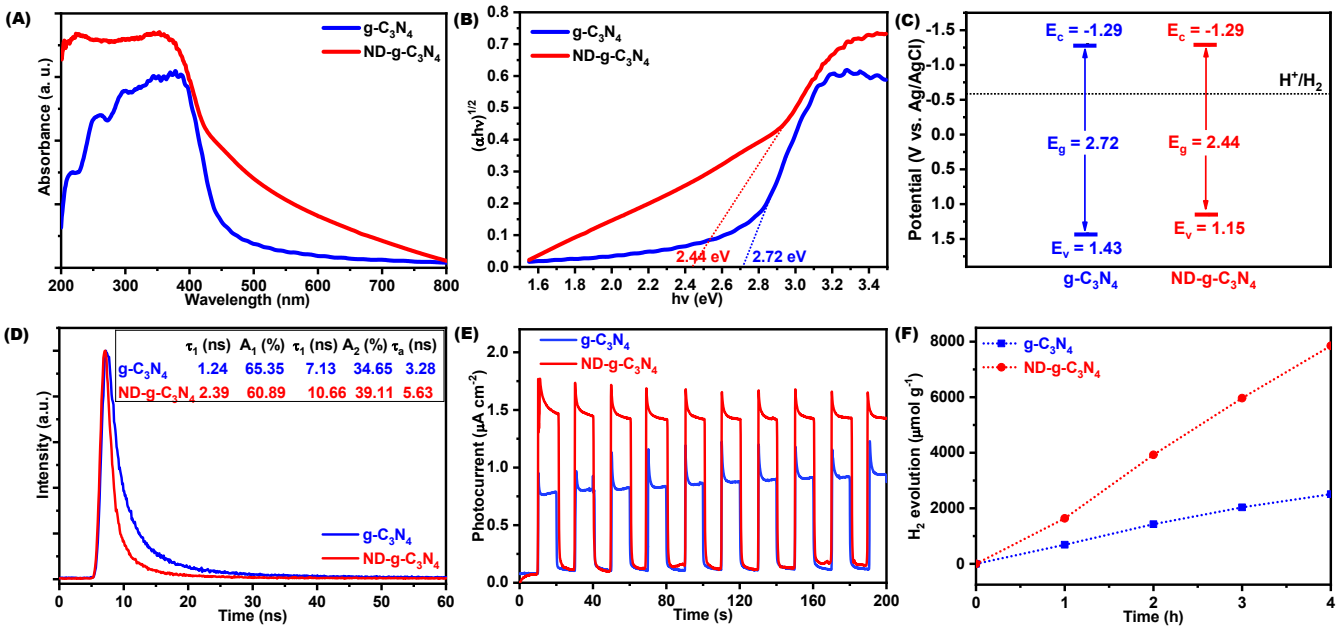

Figure 3. Optical and electronic properties of g-C_3N_4 and ND-g-C_3N_4 as well as their photocatalytic performance. (A) UV-Vis diffuse reflectance spectra, (B)plots of transformed Kubelka–Munk function versus photon energy, (C) CB and VB positions, (D) TRFDS spectra recorded under excitation of 375 nm, (E) transient photocurrent responses, and (F) Time course of hydrogen evolution for 2 wt% Pt loaded g-C_3N_4 and ND-g-C_3N_4 under UV-Vis illumination.

reflectance spectra exhibited significant redshift in the absorption edge of ND-g-C_3N_4, compared with that of g-C_3N_4 (Figure 3A). As calculated by the transformed Kubelka-Munk function, the bandgap (E_g) narrowed from 2.72 eV for g-C_3N_4 to 2.44 eV for ND-g-C_3N_4 (Figure 3B). The Mott-Schottky plots of the two samples showed the same flat-band potentials at about −1.29 V vs. Ag/AgCl (Figure S8), thermodynamically enabling the photocatalytic H_2 evolution from H_2O.[39] The results indicated that both of them are typical n-type semiconductors with the same conduction band (E_c) position. Hence the valence band (E_v) position was calculated to be 1.43 V for g-C_3N_4 and 1.15 V for ND-g-C_3N_4 (Figure 3C). The electrochemical impedance spectroscopy (EIS) measurements showed that the radius of the semi-circular Nyquist plot for ND-g-C_3N_4 was much smaller than that of g-C_3N_4, indicating that the former had better charge transfer efficiency (Figure S9). The interfacial transition of the photogenerated charge carriers was illustrated by the time-resolved fluorescent decay spectroscopy (TRFDS) (Figure 3D). An average photoluminescence lifetime of 5.23 ns was afforded by ND-g-C_3N_4, which was much longer than that obtained by g-C_3N_4 (3.28 ns). Photoluminescence (PL) spectra of g-C_3N_4 and ND-g-C_3N_4 was collected and compared to analyze the migration, transfer, and recombination processes of photogenerated electron-hole pairs in the photocatalyst (Figure S10). Compare with g-C_3N_4, the emission peak intensity of ND-g-C_3N_4 significantly decreased, indicating the reduced recombination rate of photogenerated photogenerated electron-hole pairs within the ND-g-C_3N_4 skeleton, as as PL emission originated from the recombination of free charge carriers.[50] Hence, more opportunities could be offered by ND-g-C_3N_4 for the participation of free charges in the surface photoreaction, leading to improved photocatalytic activity.[40] As shown in Figure 3E and Figure S11, upon cycling the light on and off, the ND-g-C_3N_4 owned fast, uniform, and repeatable photo-current responses, together with much higher photocurrent (1.78 μA cm^{-2}) compared with g-C_3N_4 (1.23 μA cm^{-2}). The photocatalytic performance of the pristine g-C_3N_4 and the ND-g-C_3N_4 product was evaluated using H_2 evolution as the probe reaction. In situ loaded Pt NPs were introduced due to its high conductivity, excellent electron transport kinetics, as well as negligible overpotential.[44] Notably, under the otherwise same photocatalytic conditions, a H_2 evolution rate of 1962 μmol h^{-1} was afforded by ND-g-C_3N_4 under UV-Vis light, which was more than three times that obtained by the g-C_3N_4 precursor (625 μmol h^{-1}) (Figure 3F). The superior photocatalytic activity was attributed to the enhanced light absorption and improved charge transfer efficiencies. In addition, the Pt loaded ND-g-C_3N_4 demonstrated good recyclability, with stable H_2 evolution rates being maintained after 12 h (Figure S12).

Please do not adjust margins

Conclusions

In summary, as a 2D nanomaterial, g-C_3N_4 possesses fascinating features and shows wide applications especially in photocatalysis. However, the pristine g-C_3N_4 still suffers from some issues limited by its inherent optical properties. Introduction of N-defects proved to be an efficient approach to modify its photoelectric features but always leading to amorphous architecture in the presence of strong base. The methodology introduced in this work could afford a g-C_3N_4 product with abundant N-defects while maintaining the highly crystalline framework by using an alkaline salt with a low melting point and strong ability to create vacancies. These features of the ND-g-C_3N_4 together with hydrophilic surface structure and small particle led to improved photoelectric properties in terms of redshifted absorption edge and enhanced charge carrier separation and resulted in highly improved photocatalytic performance.

Conflicts of interest

There are no conflicts to declare.

ACKNOWLEDGMENT

The research was supported financially by the Division of Chemical Sciences, Geosciences, and Biosciences, Office of Basic Energy Sciences, US Department of Energy.

Notes and references

1. C. Tan, X. Cao, X.-J. Wu, Q. He, J. Yang, X. Zhang, J. Chen, W. Zhao, S. Han, G.-H. Nam, M. Sindoro and H. Zhang, *Chem. Rev.*, 2017, **117**, 6225-6331.
2. S. Guo, H. Zhang, Y. Chen, Z. Liu, B. Yu, Y. Zhao, Z. Yang, B. Han and Z. Liu, *ACS Catal.*, 2018, **8**, 4576-4581.
3. T. C. Siu and T. A. Su, *ACS Cent. Sci.*, 2019, **6**, 11-13.
4. H. Chen, S.-Z. Yang, Z. Yang, W. Lin, H. Xu, Q. Wan, X. Suo, T. Wang, D.-e. Jiang, J. Fu and S. Dai, *ACS Cent. Sci.*, 2020, **6**, 1617–1627.
5. J. Xia, M. Ji, J. Di, B. Wang, S. Yin, Q. Zhang, M. He and H. Li, *Appl. Catal. B-Environ.*, 2016, **191**, 235-245.
6. C. Yao, A. Yuan, Z. Wang, H. Lei, L. Zhang, L. Guo and X. Dong, *J. Mater. Chem. A*, 2019, **7**, 13071-13079.
7. J. Di, J. Xia, S. Yin, H. Xu, L. Xu, Y. Xu, M. He and H. Li, *J. Mater. Chem. A*, 2014, **2**, 5340-5351.
8. Y. Luo, Y. Yan, S. Zheng, H. Xue and H. Pang, *J. Mater. Chem. A*, 2019, **7**, 901-924.
9. H. Jin, C. Guo, X. Liu, J. Liu, A. Vasileff, Y. Jiao, Y. Zheng and S.-Z. Qiao, *Chem. Rev.*, 2018, **118**, 6337-6408.
10. L. Lin, Z. Lin, J. Zhang, X. Cai, W. Lin, Z. Yu and X. Wang, *Nat. Catal.*, 2020, DOI: 10.1038/s41929-020-0476-3.
11. H. Tong, S. Ouyang, Y. Bi, N. Umezawa, M. Oshikiri and J. Ye, *Adv. Mater.*, 2012, **24**, 229-251.
12. A. Kumar, P. Raizada, A. Hosseini-Bandegharaei, V. K. Thakur, V.-H. Nguyen and P. Singh, *J. Mater. Chem. A*, 2020, DOI: 10.1039/d0ta08384d.
13. J. Fu, J. Yu, C. Jiang and B. Cheng, *Adv. Energy Mater.*, 2018, **8**, 1701503.
14. Y. Wang, X. Wang and M. Antonietti, *Angew. Chem. Int. Ed.*, 2012, **51**, 68-89.
15. A. Thomas, A. Fischer, F. Goettmann, M. Antonietti, J.-O. Muller, R. Schlogl and J. M. Carlsson, *J. Mater. Chem.*, 2008, **18**, 4893-4908.
16. G. Liu, G. Zhao, W. Zhou, Y. Liu, H. Pang, H. Zhang, D. Hao, X. Meng, P. Li and T. Kako, *Adv. Funct. Mater.*, 2016, **26**, 6822-6829.
17. T. V. de Medeiros, A. Macina and R. Naccache, *Nano Energy*, 2020, **78**.
18. Y. Zhu, Y. Feng, S. Chen, M. Ding and J. Yao, *J. Mater. Chem. A*, 2020, DOI: 10.1039/d0ta08892g.
19. G. Dong, W. Ho, Y. Li and L. Zhang, *Appl. Catal. B-Environ.*, 2015, **174-175**, 477-485.
20. J.-W. Zhang, S. Gong, N. Mahmood, L. Pan, X. Zhang and J.-J. Zou, *Appl. Catal. B-Environ.*, 2018, **221**, 9-16.
21. D. H. Wang, J. N. Pan, H. H. Li, J. J. Liu, Y. B. Wang, L. T. Kang and J. N. Yao, *J. Mater. Chem. A*, 2016, **4**, 290-296.
22. J. Liu, H. Wang, Z. P. Chen, H. Moehwald, S. Fiechter, R. van de Krol, L. Wen, L. Jiang and M. Antonietti, *Adv. Mater.*, 2015, **27**, 712-718.
23. G. Liu, T. Wang, H. Zhang, X. Meng, D. Hao, K. Chang, P. Li, T. Kako and J. Ye, *Angew. Chem. Int. Ed.*, 2015, **54**, 13561-13565.
24. Y. Cui, G. Zhang, Z. Lin and X. Wang, *Appl. Catal. B-Environ.*, 2016, **181**, 413-419.
25. L. Lei, W. Wang, C. Wang, H. Fan, A. K. Yadav, N. Hu, Q. Zhong and P. Müller-Buschbaum, *J. Mater. Chem. A*, 2020, DOI: 10.1039/d0ta07805k.
26. X. Wang, K. Maeda, A. Thomas, K. Takanabe, G. Xin, J. M. Carlsson, K. Domen and M. Antonietti, *Nat. Mater.*, 2008, **8**, 76.
27. J. Zhu, P. Xiao, H. Li and S. A. C. Carabineiro, *ACS Appl. Mater. Inter.*, 2014, **6**, 16449-16465.
28. S. Yu, J. Li, Y. Zhang, M. Li, F. Dong, T. Zhang and H. Huang, *Nano Energy*, 2018, **50**, 383-392.
29. Z. Zeng, Y. Su, X. Quan, W. Choi, G. Zhang, N. Liu, B. Kim, S. Chen, H. Yu and S. Zhang, *Nano Energy*, 2020, **69**.
30. Y. Zheng, L. Lin, X. Ye, F. Guo and X. Wang, *Angew. Chem. Int. Ed.*, 2014, **53**, 11926-11930.
31. G. Gao, Y. Jiao, E. R. Waclawik and A. Du, *J. Am. Chem. Soc.*, 2016, **138**, 6292-6297.
32. Q. Liu, C. Chen, K. Yuan, C. D. Sewell, Z. Zhang, X. Fang and Z. Lin, *Nano Energy*, 2020, **77**.
33. W.-J. Ong, L.-L. Tan, Y. H. Ng, S.-T. Yong and S.-P. Chai, *Chem. Rev.*, 2016, **116**, 7159-7329.
34. Y. Cui, Z. Ding, P. Liu, M. Antonietti, X. Fu and X. Wang, *Phys. Chem. Chem. Phys.*, 2012, **14**, 1455-1462.
35. Z. Zhu, C. Ma, K. Yu, Z. Lu, Z. Liu, P. Huo, X. Tang and Y. Yan, *Appl. Catal. B-Environ.*, 2020, **268**, 118432.
36. Y. Fang, X. Fu and X. Wang, *ACS Materials Letters*, 2020, DOI: 10.1021/acsmaterialslett.0c00215, 975-980.
37. A. Naseri, M. Samadi, A. Pourjavadi, A. Z. Moshfegh and S. Ramakrishna, *J. Mater. Chem. A*, 2017, **5**, 23406-23433.
38. Z. Lin and X. Wang, *Angew. Chem. Int. Ed.*, 2013, **52**, 1735-1738.
39. S. Yang, Y. Gong, J. Zhang, L. Zhan, L. Ma, Z. Fang, R. Vajtai, X. Wang and P. M. Ajayan, *Adv. Mater.*, 2013, **25**, 2452-2456.
40. H. Yu, R. Shi, Y. Zhao, T. Bian, Y. Zhao, C. Zhou, G. I. N. Waterhouse, L.-Z. Wu, C.-H. Tung and T. Zhang, *Adv. Mater.*, 2017, **29**, 1605148.
41. P. Niu, L. Zhang, G. Liu and H.-M. Cheng, *Adv. Funct. Mater.*, 2012, **22**, 4763-4770.
42. A. Indra, A. Acharjya, P. W. Menezes, C. Merschjann, D. Hollmann, M. Schwarze, M. Aktas, A. Friedrich, S. Lochbrunner, A. Thomas and M. Driess, *Angew. Chem. Int. Ed.*, 2017, **56**, 1653-1657.

This journal is © The Royal Society of Chemistry 20xx

Please do not adjust margins

43. P. Niu, G. Liu and H.-M. Cheng, *J. Phys. Chem. C*, 2012, **116**, 11013-11018.
44. P. Niu, L.-C. Yin, Y.-Q. Yang, G. Liu and H.-M. Cheng, *Adv. Mater.*, 2014, **26**, 8046-8052.
45. J. Chen, Z. Mao, L. Zhang, D. Wang, R. Xu, L. Bie and B. D. Fahlman, *ACS Nano*, 2017, **11**, 12650-12657.
46. J. P. Pender, J. V. Guerrera, B. R. Wygant, J. A. Weeks, R. A. Ciufo, J. N. Burrow, M. F. Walk, M. Z. Rahman, A. Heller and C. B. Mullins, *ACS Nano*, 2019, **13**, 9279-9291.
47. L. Lin, Z. Yu and X. Wang, *Angew. Chem. Int. Ed.*, 2019, **58**, 6164-6175.
48. T. Sano, S. Tsutsui, K. Koike, T. Hirakawa, Y. Teramoto, N. Negishi and K. Takeuchi, *J. Mater. Chem. A*, 2013, **1**, 6489-6496.
49. J. Liu, T. Zhang, Z. Wang, G. Dawson and W. Chen, *J. Mater. Chem.*, 2011, **21**, 14398-14401.
50. W. Zhang, L. Zhou and H. Deng, *J. Mol. Catal. A: Chem.*, 2016, **423**, 270-276.

This journal is © The Royal Society of Chemistry 20xx

Please do not adjust margins